

H-MODE TURBULENCE, POWER THRESHOLD, ELM, AND PEDESTAL STUDIES IN NSTX

R. Maingi 1), C.E. Bush 1), E.D. Fredrickson 2), D.A. Gates 2), S.M. Kaye 2), B.P. LeBlanc 2), J.E. Menard 2), H. Meyer 3), D. Mueller 2), N. Nishino 4), A.L. Roquemore 2), S.A. Sabbagh 5), K. Tritz 6), S.J. Zweben 2), M.G. Bell 2), R.E. Bell 2), T. Biewer 2), J.A. Boedo 7), D.W. Johnson 2), R. Kaita 2), H.W. Kugel 2), R.J. Maqueda 8), T. Munsat 2), R. Raman 9), V.A. Soukhanovskii 10), T. Stevenson 2), D. Stutman 6)

- 1) Oak Ridge National Laboratory, Oak Ridge TN, 37831 USA
- 2) Princeton Plasma Physics Laboratory, PO Box 451, Princeton, NJ, 08543 USA
- 3) Euratom-UKAEA Fusion Energy Association, Culham, Oxfordshire, U.K.
- 4) Hiroshima, University, Hiroshima, Japan
- 5) Columbia University, New York, NY, USA
- 6) Johns Hopkins University, Baltimore, MD, USA
- 7) University of California at San Diego, San Diego, CA USA
- 8) Nova Photonics, Princeton, NJ, USA
- 9) Univ. of Washington, Seattle, WA, USA
- 10) Lawrence Livermore National Laboratory, Livermore, CA USA

Abstract. H-mode operation plays a crucial role in NSTX research, allowing higher beta limits due to reduced plasma pressure peaking, and long pulse operation due to high bootstrap current fraction. Here, new results are presented in the areas of edge localized modes (ELMs), H-mode pedestal physics, L-H turbulence, and power threshold studies, ELMS of several other types (as observed in conventional aspect ratio tokamaks) are often observed: 1) large, Type I ELMs, 2) “medium” Type II/III ELMs, and 3) giant ELMs which can reduce stored energy by up to 30% in certain conditions. In addition, many high performance discharges in NSTX have tiny ELMs (newly termed Type V), which have some differences as compared with ELM types in the published literature. The H-mode pedestal typically contains between 25-33% of the total stored energy, and the NSTX pedestal energy agrees reasonably well with a recent international multi-machine scaling. We find that the L-H transition occurs on a ~ 100 μ sec timescale as viewed by a gas puff imaging diagnostic, and that intermittent quiescent periods precede the final transition. A power threshold identity experiment between NSTX and MAST shows comparable loss power at the L-H transition in balanced double-null discharges. Both machines require more power for the L-H transition as the balance is shifted toward lower single null. High field side gas fueling enables more reliable H-mode access, but does not always lead to a lower power threshold e.g. with a reduction of the duration of early heating. Finally the edge plasma parameters just before the L-H transition were compared with theories of the transition. It was found that while some theories can separate well-developed L- and H-mode data, they have little predictive value.

The National Spherical Torus Experiment (NSTX) is a medium-size, low aspect ratio spherical torus[1] with both neutral beam (NBI) and radio-frequency (RF) auxiliary heating, and main parameters: $R=0.86\text{m}$, $a=0.67\text{m}$, $R/a \geq 1.26$, $B_t \leq 0.6\text{ T}$, $I_p \leq 1.5\text{ MA}$, $P_{\text{NBI}} \leq 7.4\text{ MW}$, $P_{\text{RF}} \leq 6\text{ MW}$. An assessment of the attractiveness of the spherical torus (ST) concept in the areas of high beta (β) stability, turbulence and transport, start-up and current drive, and boundary physics is the main research goal of NSTX. This paper describes H-mode physics research in NSTX with the primary focus on imaging of edge-localized modes (ELMs) with new diagnostics; an overview of recent NSTX results is given in [2].

I. Edge localized modes

Several ELM types from the higher aspect ratio tokamaks have been observed on NSTX. The large ELMs with stored energy drop between 5-15% were observed at high normalized beta (β_N) ≤ 6 in lower-single null (LSN) divertor configuration and over a wider range of β_N in double-null divertor configuration (DN). An ELM, which has characteristics of both Type II and Type III ELMs from the literature, was observed in discharge shapes close to and including balanced DN. A new small ELM (termed Type V[3] since the numeral IV was used by the DIII-D group in the mid-1990's) was observed over a broad range in β_N and beta poloidal (β_p), almost exclusively in a lower-single null configuration while using the center stack midplane gas injector. Characteristics of these ELMs are presented below.

I. 1. Large ELM characteristics

Large ELMs were observed both in LSN and DN configurations with heating power well above the L-H power threshold; these ELMs share many characteristics of Type I ELMs from the literature.

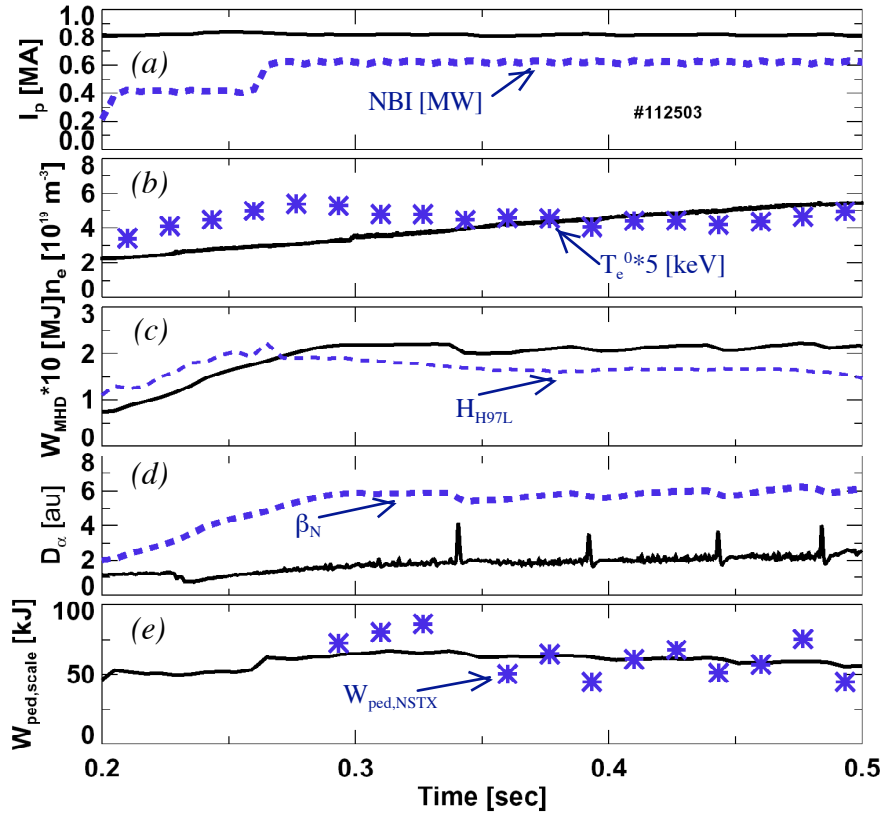


Fig. 1 – Example of a Type I ELMy discharge: (a) I_p and P_{NBI} , (b) \bar{n}_e and central T_e , (c) stored energy (W_{MHD}) and confinement relative to ITER-97 L-mode scaling (H_{H97L}), (d) D_α and \square_N , and (e) comparison of pedestal stored energy (blue data points) with an international scaling. Panel (e) is discussed in section II.

X-ray USXR) array data[5], it is reasonably clear that the perturbation propagated inwards from the edge (as opposed to a core mode e.g. sawtooth with an outward propagation)[6].

A fast visible camera (10-100 \square sec exposure, 1 msec between frames) with a fisheye view of the entire plasma column was used to image the perturbation during various ELM crashes, including these large ELMs (Fig. 2). The image of the ELM crash is consistent with a low- n (perhaps $n=1$) kink (where n is the toroidal mode number). Preceding the crash, The Mirnov coil array reveals a rapidly growing pre-cursor (growth time ≤ 100 \square sec) with intermediate mode number $5 \leq n \leq 8$.

High speed movies of the radial vs. poloidal structure of the edge turbulence during these large ELMs have been made using the gas puff imaging (GPI) technique[7,8]. The images are typically filtered for D_α light with a sight-line

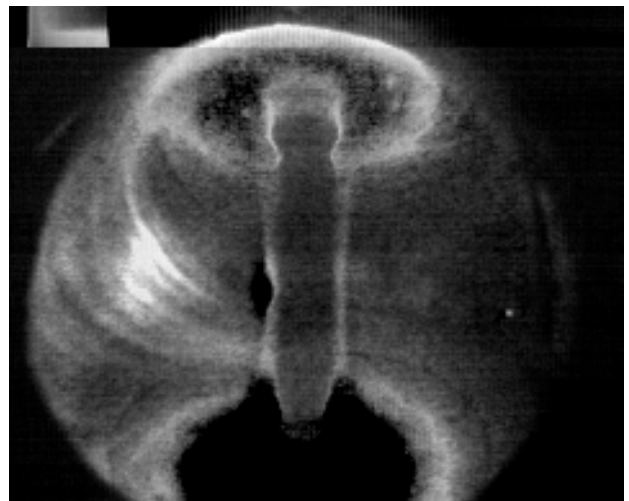


Fig. 2 – Fisheye camera image (contrast enhanced) of unfiltered light during a large ELM crash with time slice subtraction (#112503, 515msec – 510 msec).

An example of a LSN discharge with large ELMs (and also smaller Type V ELMs in-between) with frequency ~ 20 Hz is shown in Figure 1. The ion grad-B drift was toward the lower X-point. The frequency of the large ELMs generally increased with the heating power in a controlled scan, whereas the amplitude was not strongly affected. These large ELMs disappeared completely below 4 MW of NBI power for these discharge conditions. The edge n_e was typically strongly reduced during a large ELM, whereas the effect on the T_e profile is more global[4], with $\square T_e^0 \sim \square T_e^{ped}$. From ultra-soft

aligned with the typical field line pitch near the outer midplane, allowing an end-on view of the turbulent structures. Figure 3 shows a sequence of 98 images with 16 μ sec framing time during a typical large ELM, which lasted for 2 msec on the fast divertor D_{\square} channel. Note that the discharge shown in this figure was nearly identical to the one shown in Figure 1. The divertor D_{\square}

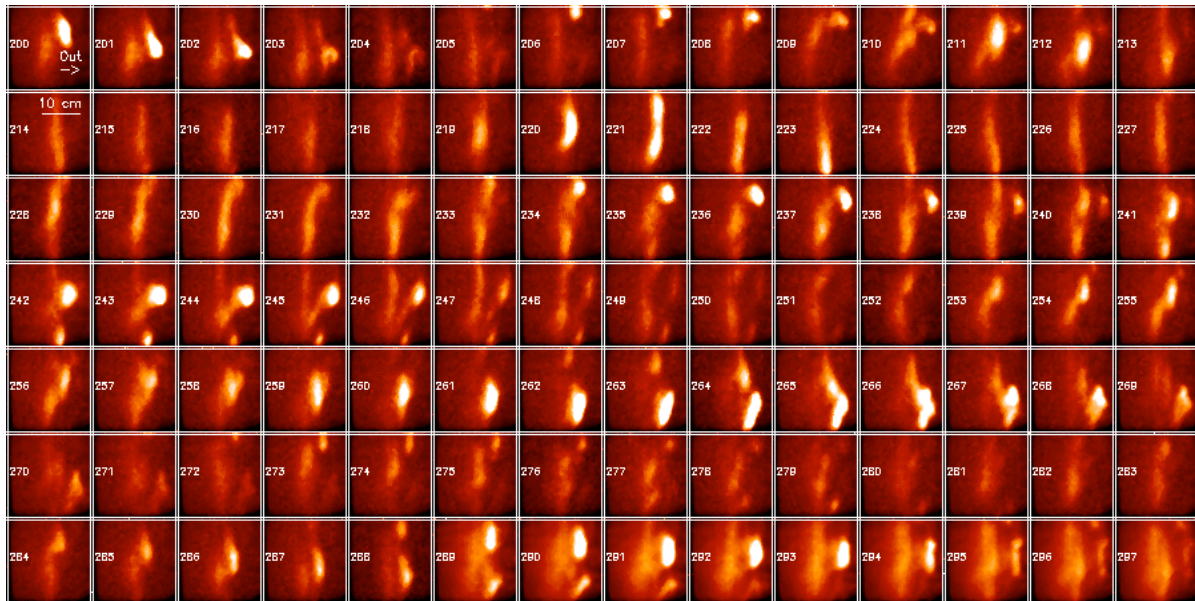


Fig. 3 – GPI image at the outer midplane of a type I ELM (#113417, 16 μ sec framing time, from 350.2 msec-351.7 msec). Spatial scale is 25 cm square.

began to increase at frame #212, peaked at frame #229, and had not recovered to baseline value by the end of the GPI sequence. This set of discharges exhibited turbulence structures on the GPI images in the interval between both large ELMs and Type V ELMs, e.g. the frames 200-202 in Figure 3 (there were no Type V ELMs in this image sequence). However the frequency of the GPI perturbations increased substantially during the ELM. Indeed the image sequence appears most similar to L-modes reported previously[8]. In addition the impact of the ELM on the divertor plasma was imaged with the tangential fast visible camera diagnostic[5, 9]. The unfiltered and D_{\square} -filtered divertor light images showed the presence of a MARFE-structure (MARFE: Multifaceted Axisymmetric Radiation from the Edge[10,11]) at the inner target between large ELMs, which was dissipated during the ELM crash[12]. The presence of the divertor MARFE is consistent with the observation[13] of detachment at the inner divertor target over much of the NSTX H-mode operational space. The divertor MARFE reformed within 10msec after the end of each large ELM.

Finally, we summarize the results of a Type I size scaling study in DN configuration[14]. The size of large ELMs was measured as a fraction of either the total or the pedestal stored energy lost during

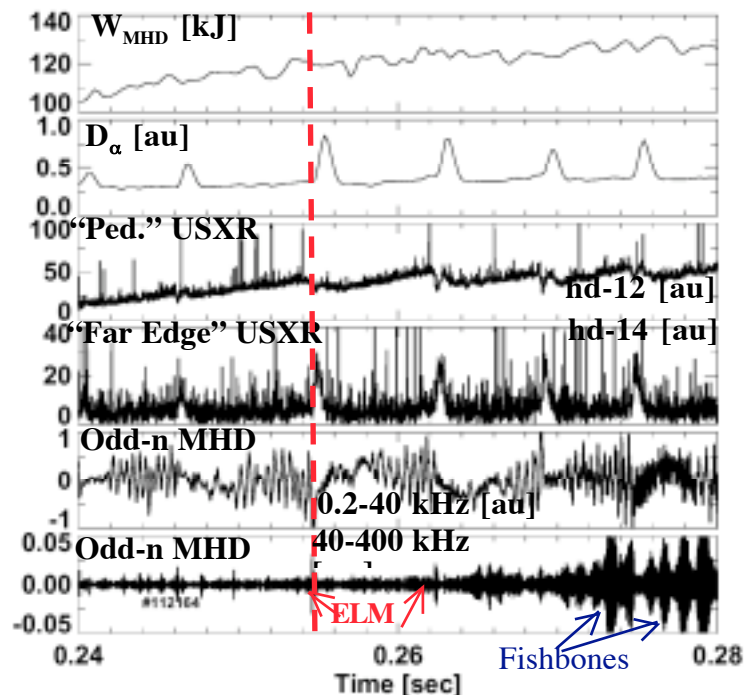


Fig. 4 – discharge with Type III/III ELMs. The dashed line indicates time of a single Type III ELM, but several others are observed within the frames.

the ELM, with a range up to 8% for total stored energy loss fraction and 30% pedestal loss fraction. It was found that the size of the ELMs decreased by both measures with increasing density, as observed at conventional aspect ratio. Even larger ELMs were observed in LSN configuration, with a total stored energy loss fraction up to 30%. Indeed one must question whether such global perturbations should even be called ELMs, but the inward propagation direction is relatively clear from USXR data. The physics of these giant events and the probable mode coupling are being investigated.

I. 2. Medium ELM characteristics

A smaller ELM was observed (e.g. Fig. 4) in discharges with a shape near double-null (i.e. the physical separation of the X-points mapped to the outer midplane ($drsep$) ≤ 1 cm, with the magnetic balance favoring the lower X-point) and also in a balanced double-null. For the biased-



Fig. 5 – Fisheye camera image (contrast enhanced) of D_{α} light during a Type III/III ELM crash with time slice subtraction (#113409, 385msec – 390 msec).

downward shape, the ELMs were observed only in the vicinity of the L-H power threshold and the frequency increased as the density ramped upward through the discharge. Accompanying the density ramp was a radiated power increase and a decrease in the scrape-off layer (SOL) loss power. Increasing the NBI power resulted in less frequent ELMs until this particular kind of ELM disappeared. Hence the data indicate an inverse dependence of the ELM frequency on SOL loss power and appearance near the power threshold, consistent with Type III ELMs[15]. However the shape dependence is suggestive of Type II ELMs [16], hence the ambiguity in a clear identification.

number $n=1$ (but occasionally $n=2-3$) appeared for several msec before the ELM crash, e.g. panel 4e. The ELM crash itself was observed in the high frequency integrated Mirnov signals in panel 4f. The fisheye plasma TV usually showed an intermediate- n (i.e. clearly not $n=1$, but perhaps $n=3$ or $n=4$) perturbation during the ELM crash (Fig. 5). GPI images of these ELMs showed a less dramatic turbulence increase during the crash, consistent with a smaller event. The divertor fast camera images showed[12] a cyclical behavior in which the divertor MARFE either migrated to the inner midplane or dissipated during the magnetic pre-cursor, and was re-established following the ELM pulse. These ELMs did not burn through the divertor MARFE near the inner target.

I. 3. Tiny ELM characteristics

The smallest ELMs observed in NSTX are observed over a wide operational window:

Figure 4 shows an inversion of the USXR pulse associated with the ELM, between chords 12 and 14, i.e. localized to the edge. A very clear pre-cursor with frequency ~ 2 kHz and usually mode

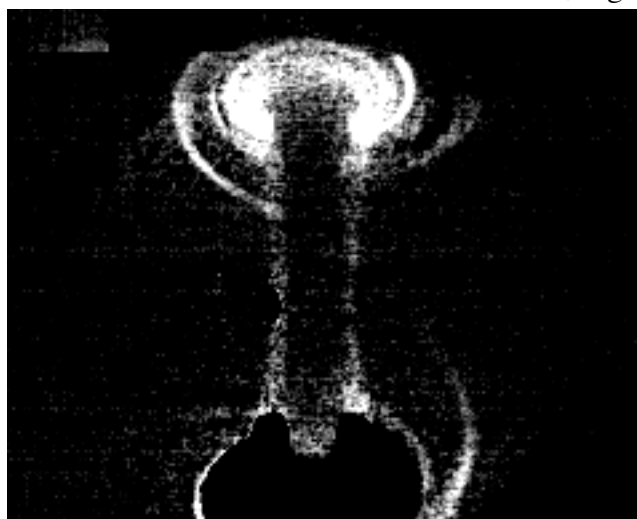


Fig. 6 – Fisheye camera image (contrast enhanced) of unfiltered light during a Type V ELM crash with time slice subtraction (#113024, 520msec – 515 msec).

$3 \times 10^{19} \text{ m}^{-3} < \bar{n}_e < 6 \times 10^{19} \text{ m}^{-3}$, $2.5 \leq \beta_N \leq 6$ and $0.5 \leq \beta_p \leq 1.5$, and they have been named Type V[3]. An example of a discharge with these tiny ELMs occurring between large Type I ELMs is shown in Figure 1; the tiny ELMs appear as “hash” on the divertor D_{\square} . The ELMs usually



Fig. 7 – view of NSTX lower divertor region, with approximate tangential sight-line of fast divertor camera.

appear as single peaks on the fastest divertor D_{\square} channel and on the edge USXR data. There was no clear effect on the stored energy, down to the EFIT reconstruction[17, 18] statistical resolution of +/-1.5% at the fastest reliable resolution time of 0.25 msec. A short-lived $n=1$ pre-cursor oscillation was evident before the ELM crash, persisting for up to 2 toroidal transits before the crash and disappearing between ELMs. The pre-cursor propagated in the counter- I_p direction.

The fisheye plasma TV showed a picture of a very localized perturbation during a tiny ELM, possibly the illumination up of a narrow flux tube (Fig. 6). GPI images of these ELMs showed only a modest difference between the ELM and the background turbulence.

Finally the divertor visible camera showed each Type V ELM clearly. The divertor camera sightline is shown in Figure 7, and data during a tiny ELM are displayed in Figure 8. Very small vertical oscillations in the position of the divertor MARFE occur during each ELM, and conspicuous finger-like structures evolved in the vicinity of the X-point. The tiny ELM perturbation typically lasted for 400 μ sec on the divertor camera images.

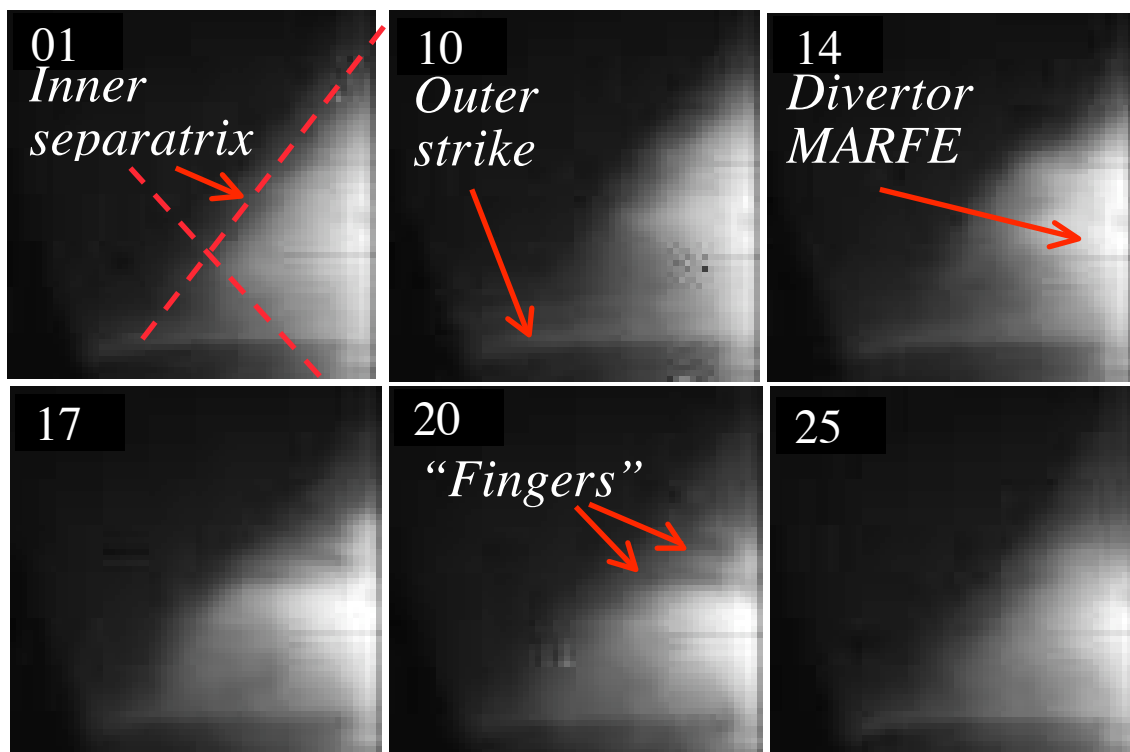


Fig. 8 – divertor camera images of unfiltered light during a Type V ELM (#112503 @ 0.398 sec). The relative frame numbers are indicated and the time between frames is 24.7 μ sec. The perturbation persists for ~ 400 μ sec.

In comparison to the behavior of small ELMs reported by conventional aspect ratio devices, these events are most similar to the “grassy” ELMs reported during high recycling steady (HRS) mode operation on JFT-2M[19]. However we note that there is no evidence of a quasi-coherent mode as observed on JFT-2M and also during the Enhanced D₀ H-mode in C-MOD[20], nor is there any evidence of an edge harmonic oscillation as observed during quiescent H-mode in DIII-D[21, 22]. The edge particle transport was clearly enhanced during these events, as indicated by broadening of the edge carbon density profiles from charge-exchange recombination spectroscopy, as well as direct detection of particle flux by a reciprocating fast-stroke probe. The question remains, however, whether the enhanced edge particle transport due to these events would be sufficient for density control if an in-vessel pumping system were introduced into NSTX.

II. H-mode pedestal scaling

The presence of an edge pedestal is most obvious in the flat or slightly hollow edge n_e profiles in NSTX, and to a lesser extent in the edge P_e profiles. The edge T_e profile does not usually exhibit a large, obvious pedestal. All three profiles near the outer midplane were fitted with a (“standard”) modified hyperbolic tangent fitting function[23], including a linear term for the profile inside the pedestal. The spatial resolution of the NSTX Thomson system (60 Hz, 20 spatial chords, outer edge resolution 2-3 cm) allows reasonable determination (i.e. to within +/- 20%) of the pedestal heights in certain shapes, but not the widths and gradients directly from the data (although estimates can be obtained from the spline fits to the data). From the tanhfits, the NSTX pedestal n_e , T_e , and P_e are typically in a range between 2 and 5 $\times 10^{19}$ m⁻³, 100 and 300 eV, and 1 and 3 kPa respectively.

The pedestal stored energy was obtained[24] from the fitted pedestal pressure with the relation $W_{ped} = 0.92 \cdot \text{volume}_{EFF} \cdot p_e^{ped} \cdot 3$, i.e. implicitly assuming $T_i^{ped} = T_e^{ped}$. The factor of 0.92 is based on the observation that the steep gradient region of the pedestal profiles lies on closed field lines, i.e. the pedestal parameters do not encompass the entire plasma volume [25]. This analysis showed that the NSTX pedestal typically contains between 25-33% of the total plasma stored energy. A comparison of this pedestal stored energy with the multi-machine scaling relation[24] $W_{ped, scale} [MJ] = 0.0064 \times I_p^{1.58} R^{1.08} P_{heat}^{0.42} n_e^{-0.08} B_t^{0.06} \bar{\nu}^{1.81} (a/R)^{-2.13} M^{0.2} (q_{95}/q_{cyl})^{2.09}$ is shown in Figure 1 for the previously discussed NSTX LSN discharge with mixed Type I and Type V ELMs. For reference, the scaling was a regression fit to data from the ASDEX Upgrade, C-MOD, DIII-D, JET, JFT2M, JT-60U, and MAST devices. It can be seen in panel (e) that the NSTX fitted pedestal values generally lay within +/- 25% of the scaling. Thomson pulses just after large ELMs lay below the scaling, whereas the data far away from the large ELMs lay above the scaling.

III. L-H transition studies

Several experiments and analysis have been conducted in the L-H transition physics area, including imaging of turbulence at the transition, an L-H power threshold identity experiment in conjunction with the Mega-Amp Spherical Tokamak (MAST) at Culham, U.K., an experiment to determine the effect of poloidal fueling location on power threshold, and a comparison of the edge parameters and gradients with theories of the L-H transition. Each of these is discussed below.

Transitions from L-mode to H-mode were imaged with the GPI diagnostic, and they appeared as a smooth evolution from a turbulent state to a quiescent state over a timescale ≤ 100 μ s, as illustrated in frames #136-151 of Figure 9. This transition apparently proceeded without any new spatial features or flows, i.e. with little or no increase in the poloidal flow shear or shape or of the turbulent fluctuations (at least, as visible to the eye). We note, however, that the radial depth illuminated by the GPI diagnostic is limited by the penetration depth of deuterium neutrals, and that flow changes predicted by some theories could have occurred deeper into the plasma. The main L-H transition was sometimes preceded by transient periods of H-mode-like quiescence, as if the transition were ‘dithering’ for up to ≈ 5 msec before being completed. Transitions from H-L generally appeared as ≈ 5 -10 cm sized poloidal perturbations, which evolved rapidly (≤ 100 μ sec) into radially moving blobs characteristic of L-mode turbulence.

The influence of magnetic balance was investigated in an L-H power threshold identity experiment with the MAST device. Both NSTX and MAST were operated with similar engineering parameters and in similar shapes: $I_p = 0.5$ MA, $B_t = 0.45$ T, $a \sim 0.6-0.63$ m, $\kappa = 1.8$, $\beta = 0.45$, with center stack midplane gas fueling, largely inductive I_p ramp-up, and NBI heating after I_p flat-top. In balanced DN, the LH transition power was between 500-600 kW in both machines[26]. As the magnetic balance was varied, favoring the lower divertor, the power threshold increased in MAST and an H-mode transition was not obtained in NSTX, confirming previous MAST results[27] that the power threshold has a minimum near balanced double-null. This minimum could be a local minimum, however, as the absolute lowest power threshold in NSTX is obtained in lower-single null configuration, with ready access to ohmic H-mode [28].

Both MAST and NSTX have previously reported that fueling from the center stack region facilitated H-mode access[29,30], as compared with low-field side fueling. The improved access was explained by a revision to neoclassical theory [31] to account for a poloidal neutral fueling profile on the momentum balance. The basic theory prediction is that toroidal rotation and E_r

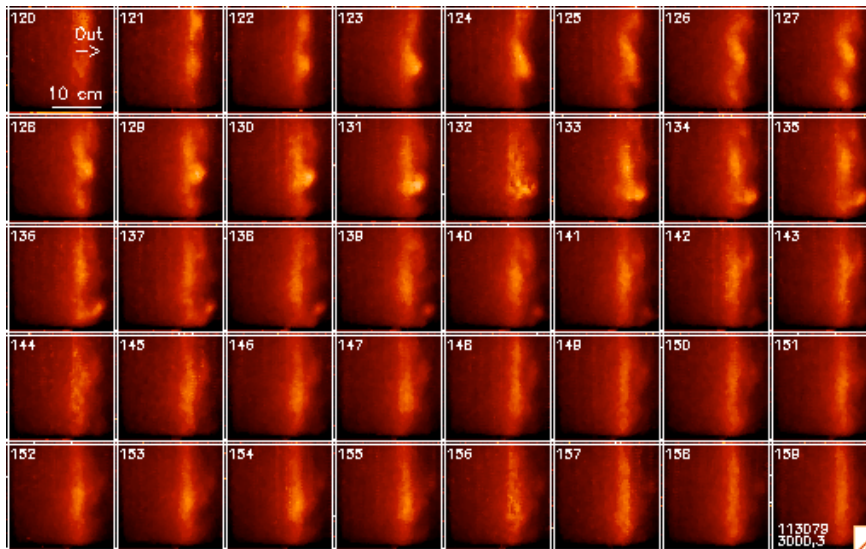


Fig. 9 – Edge turbulence during an L-H transition as viewed by the GPI diagnostic in the radial (left-right) vs. poloidal (up-down) plane for #113079. The transition occurs between frames #136-151. Here the framing rate is 4 μ sec/frame and the field of view is 24 cm x 24 cm.

should be higher with high-field side fueling due to reduced absolute charge-exchange loss of momentum. The MAST data were semi-quantitatively consistent with the theory [32], whereas the NSTX data with early NBI heating were qualitatively consistent with the theory [33]. However more recent NSTX experiments have shown that the improved H-mode access did not always translate to a reduced power threshold and larger E_r as the duration of the early NBI heating phase was reduced; indeed, discharges with power

threshold within 20% were obtained with high-field side and low-field side (LFS) fueling. Nonetheless LFS fueling was successfully used to inhibit the L-H transition for other experiments requiring L-mode conditions in NSTX, suggesting that the gas fueling location is not the sole cause of improved H-mode access.

Finally we compared[34] edge plasma parameters with several theories of the L-H transition. Edge parameters were obtained from the NSTX Thomson scattering system. Due to the limited spatial resolution, the gradients were obtained from a cubic spline fit to the data. The clearest pedestal was typically observed in the n_e profile, and the edge gradients were evaluated in the middle of the steep n_e gradient region. Most of the theories clearly separated the well developed L and H-mode data points (most notably with the MHD ballooning parameter $\beta_{MHD} = -Rq^2 d\beta/dr$)[35]. However those theories were unable to separate points *just* before and after the transition, indicating little predictive capability. This study also suggested that fast ion loss at low I_p may be responsible[34] for the apparent I_p dependence of the LH threshold reported previously[4].

IV. Summary

Substantial progress was made in ELM research, in particular imaging of ELMs with new diagnostics. We find that several of the ELM types reported by conventional aspect ratio devices have strong similarities to ones observed in NSTX. The small ELMs in NSTX uniformly have

low-n pre-cursors, whereas the larger ELMs have intermediate-n pre-cursors. As may be expected, the large ELMs cause the inner divertor plasma to re-attach transiently, whereas the smaller ELMs are absorbed by the divertor MARFE near the inner target.

Progress was also made on pedestal physics and L-H transition research. The stored energy in the NSTX pedestal agrees reasonably well with a multi-machine international scaling (which notably includes data from the low aspect ratio MAST device). Images of the L-H transition showed a continuous process without apparent generation of new flows. Finally the L-H power threshold in NSTX and MAST was comparable in DN configuration, indicating that differences in the wall proximity between the two machines did not have a substantial impact on the power threshold.

Acknowledgements

This research was supported by the U. S. Dept. of Energy under contracts DE-AC05-00OR22725, DE-AC02-76CH03073, DE-AC04-94AL85000, W-7405-ENG-36, W-7405-ENG-48 and grants DE-FG02-99ER54524 and DE-FG02-99ER54523. We gratefully acknowledge the contribution of the NSTX technical staff and neutral beam operations staff.

References

- 1 M. Ono, et. al., *Nuclear Fusion* **40**, (2000)557.
- 2 S. M. Kaye, et. al., this conference, paper OV/2-3.
- 3 R. Maingi, et. al., *Nuclear Fusion* submitted, (2004).
- 4 C. E. Bush, et. al., *Physics of Plasmas* **10**, (2003)1755.
- 5 D. Stutman, et. al., *Review of Scientific Instruments* **74**, (2003)1982.
- 6 K. Tritz, et. al., Presented at the APS meeting on Plasma Physics, Jeckyll Island, GA, Oct. 15-19, 2004.
- 7 R. J. Maqueda, et. al., *Review of Scientific Instruments* **74**, (2003)2020.
- 8 S. J. Zweben, et. al., *Nuclear Fusion* **44**, (2004)134.
- 9 A. L. Roquemore, et. al., *Review of Scientific Instruments* at press., (2004).
- 10 B. Lipshultz, et. al., *Nuclear Fusion* **24**, (1984)977.
- 11 D. R. Baker, et. al., *Nuclear Fusion* **22**, (1982)807.
- 12 R. Maingi, et. al., Proc. 31st EPS Conference on Plasma Physics and Contr. Fusion, London, U.K., June 28-July 2, 2004 28G, (2004)Paper P2.189.
- 13 V. A. Soukhanovskii, et. al., *J. Nucl. Materials* at press.
- 14 R. Maingi, et. al., *J. Nucl. Materials*, (at press).
- 15 E. J. Doyle, et. al., *Physics of Fluids B* **3**, (1991)2300.
- 16 T. Ozeki, et. al., *Nuclear Fusion* **30**, (1990)1425.
- 17 L. L. Lao, et. al., *Nuclear Fusion* **25**, (1985)1611.
- 18 S. A. Sabbagh, et. al., *Nuclear Fusion* **41**, (2001)1601.
- 19 K. Kamiya, et. al., *Nuclear Fusion* **43**, (2003)1214.
- 20 Y. Takase, et. al., *Physics of Plasmas* **4**, (1997)1647.
- 21 C. M. Greenfield, et. al., *Physical Review Letters* **86**, (2001)4544.
- 22 K. H. Burrell, et. al., *Physics of Plasmas* **8**, (2001)2153.
- 23 R. J. Groebner, et. al., *Plasma Physics Controlled Fusion* **40**, (1998)673.
- 24 J. G. Cordey, et. al., *Nuclear Fusion* **43**, (2003)670.
- 25 K. Thomsen, et. al., *Plasma Physics Controlled Fusion* **44**, (2002)A429.
- 26 H. Meyer, et. al., this conference, paper EX/P3-8.
- 27 H. Meyer, et. al., *Plasma Physics Controlled Fusion* **46**, (2004)A291.
- 28 C. E. Bush, et. al., Proc. of 10th US-EU TTF Workshop, Varenna, Italy, Sept. 6-9, 2004.
- 29 A. R. Field, et. al., *Plasma Physics Controlled Fusion* **44**, (2002)A113.
- 30 R. Maingi, et. al., *Nuclear Fusion* **43**, (2003)969.
- 31 P. Helander, et. al., *Physics of Plasmas* **10**, (2003)4396.
- 32 A. R. Field, et. al., *Plasma Physics Controlled Fusion* **46**, (2004)981.
- 33 R. Maingi, et. al., *Plasma Physics Controlled Fusion* **46**, (2004)A305.
- 34 S. M. Kaye, et. al., *Physics of Plasmas* **10**, (2003)3953.
- 35 B. N. Rogers, et. al., *Physical Review Letters* **81**, (1998)4396.